

A Numerical Study of Magnetic Reconnection: A Central Scheme for Hall MHD

Xin Qian, Jorge Balbás, Amitava Bhattacharjee, and Hongang Yang

ABSTRACT. Over the past few years, several non-oscillatory central schemes for hyperbolic conservation laws have been proposed for approximating the solution of the Ideal MHD equations and similar astrophysical models. The simplicity, versatility, and robustness of these *black-box* type schemes for simulating MHD flows suggest their further development for solving MHD models with more complex wave structures. In this work we construct a non-oscillatory central scheme for the Hall MHD equations and use it to conduct a study of the magnetic reconnection phenomenon in flows governed by this model.

1. Introduction

The successful implementation of non-oscillatory central schemes for the equations of ideal magnetohydrodynamics (MHD) and similar astrophysical models (see, for example, [3, 2, 9]), and the versatility of these *black-box* type schemes, suggest their further development for computing the approximate solutions of other MHD models whose more complex characteristic decomposition makes the utilization of schemes based on Riemann solvers impractical. In this work, we present a high-resolution, non-oscillatory, central scheme for the the Hall MHD model

$$(1.1a) \quad \frac{\partial \rho}{\partial t} = -\nabla \cdot (\rho \mathbf{v})$$

$$(1.1b) \quad \frac{\partial}{\partial t} (\rho \mathbf{v}) = -\nabla \cdot \left\{ \rho \mathbf{v} \mathbf{v}^\top + \left(p + \frac{B^2}{2} \right) I_{3 \times 3} - \mathbf{B} \mathbf{B}^\top \right\}$$

$$(1.1c) \quad \frac{\partial \mathbf{B}}{\partial t} = -\nabla \times \mathbf{E}$$

$$(1.1d) \quad \frac{\partial U}{\partial t} = -\nabla \cdot \left\{ \left(U + p - \frac{B^2}{2} \right) \mathbf{v} + \mathbf{E} \times \mathbf{B} \right\},$$

where (1.1a), (1.1b), and (1.1d) express the conservation of mass, momentum and energy respectively, and equation (1.1c) the evolution of the magnetic field, which

1991 *Mathematics Subject Classification*. Primary 76W05, 76M12; Secondary 65Z05.

Key words and phrases. MHD, Central Schemes, Reconnection.

also implies the solenoidal constraint,

$$(1.2) \quad \nabla \cdot \mathbf{B} = 0.$$

The total energy, U , momentum, $\rho \mathbf{v}$, and magnetic field, \mathbf{B} , are coupled through the equation of state,

$$(1.3) \quad U = \frac{p}{\gamma - 1} + \frac{\rho v^2}{2} + \frac{B^2}{2}.$$

And the electric field, \mathbf{E} , is expressed in the generalized Ohm's law

$$(1.4a) \quad \mathbf{E} = -\mathbf{v} \times \mathbf{B} + \eta \mathbf{j} + \frac{\delta_i}{L_0} \frac{\mathbf{j} \times \mathbf{B}}{\rho} - \frac{\delta_i}{L_0} \frac{\nabla \bar{\mathbf{p}}}{\rho} + \left(\frac{\delta_e}{L_0} \right)^2 \frac{1}{\rho} \left[\frac{\partial \mathbf{j}}{\partial t} + (\mathbf{v} \cdot \nabla) \mathbf{j} \right],$$

$$(1.4b) \quad \mathbf{j} = \nabla \times \mathbf{B}$$

where L_0 is the normalizing length unit, and δ_e and δ_i stand for the electron and ion inertia respectively; they are related to the electron-ion mass ratio by $(\delta_e/\delta_i)^2 = m_e/m_i$. For the simulations considered in this work, the electron pressure tensor, $-(\delta_i/L_0)(\nabla \bar{\mathbf{p}}/\rho)$ can be ignored.

This model follows from the MHD equations after normalizing as the Geospace Environment Modeling (GEM) challenge, preserving the unit length in the generalized Ohm's law, (1.4), for simplicity.

The scheme we propose below is built upon the semi-discrete formulation of Kurganov and Tadmor, [14], and we employ it to investigate the role that the Hall term, $\mathbf{j} \times \mathbf{B}$, and the electron inertia term,

$$(1.5) \quad T_e = \left(\frac{\delta_e}{\delta_i} \right)^2 \frac{1}{\rho} \left\{ \frac{\partial}{\partial t} + (\mathbf{v} \cdot \nabla) \right\} \mathbf{j},$$

play in the magnetic reconnection process.

Our work is organized as follows: in §2 we briefly describe the physical phenomena under consideration and the physical relevance of the terms on the right hand side of equation (1.4). In §3 we describe the proposed numerical scheme and its properties, and in §4 we present the numerical simulations calculated with the central scheme and discuss our findings.

2. Theoretical background: Magnetic Reconnection and Hall MHD

Magnetic reconnection is an irreversible process observed in space and laboratory plasma in which magnetic fields with different direction merge together and dissipate in the diffusive region breaking the magnetic frozen-in condition and quickly converting magnetic energy into kinetic and thermal energy. It is widely believed that the reconnection process is the main energy converting process in space, and most of the eruptive events are driven or associated with it.

Classic MHD theory –without the Hall term– predicts a much slower reconnection process than direct space observations suggest. Numerical simulations suggest that the Hall effect [15, 6] –caused by ions being heavier than the electrons, could enable fast reconnection, and both in-site space observation[10] and laboratory experiments[17] provide evidence of the presence of the Hall effect in the reconnection process. In addition, recent particle in cell (PIC) simulations [4, 8, 11] suggest that electron's kinetic effect might also be important in the reconnection process.

In view of these results, we investigate the ability of the model (1.1) – (1.4) to describe the reconnection phenomenon by simulating flows with different typical scales L_0 . When this is of the same order as δ_i , but still much larger than δ_e , the electron inertia term, (1.5) in the generalized Ohm law, (1.4a), may be ignored, but not the Hall term, $\mathbf{j} \times \mathbf{B}$. The magnetic frozen-in condition can no longer be satisfied where the Hall term becomes large. In this region, fluid elements don't flow along the magnetic field, instead they may move across the field lines. For those flows, we write the electric field as

$$(2.1) \quad \mathbf{E} = -\mathbf{v} \times \mathbf{B} + \frac{\mathbf{j} \times \mathbf{B}}{\rho} + \eta \mathbf{j} + \eta_j \Delta \mathbf{j}.$$

When the typical scale L_0 approaches the electron inertia length δ_e , the electron's behavior can no longer be ignored and the electron inertia term in the generalized Ohm's law, (1.4) should be include in the simulation. The electric field for this flows reads

$$(2.2) \quad \mathbf{E} = -\mathbf{v} \times \mathbf{B} + \frac{\mathbf{j} \times \mathbf{B}}{\rho} + \eta \mathbf{j} + \eta_j \Delta \mathbf{j} + T_e.$$

In both cases, the hyperresistivity, $\eta_j \Delta \mathbf{j}$ –mainly a numerical artifact– helps smoothing the structure around the grid scale without strongly diffusing the longer scale lengths.

3. Numerical Scheme

Both Hall and the electron inertia terms in (2.1) and (2.2) pose significant numerical challenges for simulating MHD flows. Unlike in classical MHD where the characteristic speeds remain constant with respect to the wave frequency, the Alfvén mode wave in Hall MHD satisfies the dispersion relation $v \sim k$ (where k is related to the wave frequency by $\omega \sim k^2$, [5]). Thus, the Alfvén wave speed increases when the wave length becomes small, $v \sim 1/\lambda$, and the maximum wave speed increases as the grid is refined, $v_{max} \sim 1/\Delta x$, requiring extremely small time steps that may result in too much numerical dissipation.

Results previously obtained with central schemes for Ideal MHD flows, [3, 2], and the minimal characteristic information from the underlying PDE they required, suggest these as the building block for new schemes to solve more complex MHD flows. In particular, we turn our attention to the semi-discrete central formulation of Kurganov and Tadmor, [14], whose numerical viscosity does not increase as the time step decreases –in contrast with fully-discrete central schemes whose viscosity is of order $\mathcal{O}((\Delta x)^{2r}/\Delta t)$, the viscosity of semi-discrete schemes is of order $\mathcal{O}((\Delta x)^{2r-1})$.

In order to construct our central scheme, we begin by re-writting the system (1.1) in conservation form,

$$(3.1) \quad u_t + f(u)_x + g(u)_y = 0,$$

with

$$(3.2a) \quad u = (\rho, \rho v_x, \rho v_y, \rho v_z, B_x, B_y, B_z, U)^\top$$

$$(3.2b) \quad f(u) = \left(\rho v_x, \rho v_x^2 + p + \frac{B^2}{2} - B_x^2, \rho v_x v_y - B_x B_y, \rho v_x v_z - B_x B_z, \right. \\ \left. 0, -E_z, E_y, U' v_x + E_y B_z - E_z B_y \right)^\top$$

$$(3.2c) \quad g(u) = \left(\rho v_y, \rho v_x v_y - B_y B_x, \rho v_y^2 + p + \frac{B^2}{2} - B_y^2, \rho v_y v_z - B_y B_z, \right. \\ \left. E_z, 0, -E_x, U' v_y + E_z B_x - E_x B_z \right)^\top,$$

where

$$(3.3) \quad U' = U + p - \frac{B^2}{2} \quad \text{and} \quad p = (\gamma - 1) \left(U - \frac{\rho v^2}{2} - \frac{B^2}{2} \right),$$

and the electric field given by (2.1) or (2.2).

3.1. Central Schemes for Hyperbolic Conservation Laws. To approximate the solution of the Hall MHD model, we construct a semi-discrete central scheme based on the formulation of Kurganov and Tadmor for hyperbolic conservation laws in 2D, [14]. A formulation that we describe here briefly for the shake of completeness.

Central schemes realized the solution of the hyperbolic conservation law in terms of the cell average of u over the control volume $I_{i,j} = [x_{i-\frac{1}{2}}, x_{i+\frac{1}{2}}] \times [y_{j-\frac{1}{2}}, y_{j+\frac{1}{2}}]$,

$$(3.4) \quad \bar{u}_{i,j}(t) = \frac{1}{\Delta x \Delta y} \int_{x_{i-\frac{\Delta x}{2}}}^{x_{i+\frac{\Delta x}{2}}} \int_{y_{j-\frac{\Delta y}{2}}}^{y_{j+\frac{\Delta y}{2}}} u(x, y, t) dy dx.$$

Integrating (3.1) over $I_{i,j}$ and dividing by the space scales Δx and Δy , yields the equivalent formulation

$$(3.5) \quad \frac{d}{dt} \bar{u}_{i,j}(t) = -\frac{1}{\Delta x \Delta y} \left[\int_{y_{j-\frac{1}{2}}}^{y_{j+\frac{1}{2}}} \left(f(u(x_{i+\frac{1}{2}}, y)) - f(u(x_{i-\frac{1}{2}}, y)) \right) dy \right. \\ \left. + \int_{x_{i-\frac{1}{2}}}^{x_{i+\frac{1}{2}}} \left(g(u(x, y_{j+\frac{1}{2}})) - g(u(x, y_{j-\frac{1}{2}})) \right) dx \right],$$

which we write in the more compact form

$$(3.6) \quad \frac{d}{dt} \bar{u}_j(t) = -\frac{1}{\Delta x} \left[H_{i+\frac{1}{2},j}^x - H_{i-\frac{1}{2},j}^x \right] - \frac{1}{\Delta y} \left[H_{i,j+\frac{1}{2}}^y - H_{i,j-\frac{1}{2}}^y \right]$$

where the numerical fluxes $H_{i\pm\frac{1}{2},j}^x$ and $H_{i,j\pm\frac{1}{2}}^y$ approximate the integrals on the right of (3.5) and are calculated so as to account for the propagation of discontinuities at the cell interfaces $x = x_{i\pm\frac{1}{2}}$ and $y = y_{j\pm\frac{1}{2}}$. For the results we presented below, we chose the midpoint rule for approximating the integrals, which results in the

fluxes,

$$(3.7a) \quad H_{i+\frac{1}{2},j}^x = \frac{f(u_{i+1,j}^W) + f(u_{i,j}^E)}{2} - \frac{a_{i+\frac{1}{2},j}^x}{2} (u_{i+1,j}^W - u_{i,j}^E)$$

$$(3.7b) \quad H_{i,j+\frac{1}{2}}^y = \frac{g(u_{i,j+1}^S) + g(u_{i,j}^N)}{2} - \frac{a_{i,j+\frac{1}{2}}^y}{2} (u_{i,j+1}^S - u_{i,j}^N).$$

For the actual implementation of the scheme, the values of $u(x, y, t)$ at the cell interfaces, $u_{i,j}^{N/S,E/W}(t)$ are recovered via a non-oscillatory, piece-wise polynomial reconstruction $R(x, y; \bar{u}(t)) = \sum_{i,j} p_{i,j}(x, y) \cdot \mathbf{1}_{I_{i,j}}(x, y)$, and defined as

$$(3.8a) \quad u_{i,j}^E := p_{i,j}(x_{i+\frac{1}{2}}, y_j) \quad u_{i,j}^W := p_{i,j}(x_{i-\frac{1}{2}}, y_j)$$

$$(3.8b) \quad u_{i,j}^N := p_{i,j}(x_i, y_{j+\frac{1}{2}}) \quad u_{i,j}^S := p_{i,j}(x_i, y_{j-\frac{1}{2}}),$$

and $a_{i+\frac{1}{2}}^x$ and $a_{i,j+\frac{1}{2}}^y$ stand for the maximum speeds of propagation at the cell interfaces in the x and y directions respectively; we approximate these by

$$(3.9) \quad a_{i+\frac{1}{2},j}^x = \max \{ \rho(u_{i+1,j}^W), \rho(u_{i,j}^E) \}, \quad a_{i,j+\frac{1}{2}}^y = \max \{ \sigma(u_{i,j+1}^S), \sigma(u_{i,j}^N) \},$$

where ρ and σ stand for the spectral radius of the jacobian matrices of $f(u)$ and $g(u)$ respectively. These values will, indeed, be exact if $f(u)$ and $g(u)$ are convex. For the second order scheme that we propose, the interface values are reconstructed from the cell averages via the bi-linear functions

$$(3.10) \quad p_{i,j}(x, y) = \bar{u}_{i,j} + (u_x)_{i,j}(x - x_i) + (u_y)_{i,j}(y - y_j)$$

with the numerical derivatives of u approximated with the limiter, [19],

$$(3.11) \quad (u_x)_{i,j} = \text{minmod} \left\{ \frac{\bar{u}_{i+1,j} - \bar{u}_{i,j}}{\Delta x}, \frac{\bar{u}_{i,j} - \bar{u}_{i-1,j}}{\Delta x} \right\},$$

and similarly for $(u_y)_{i,j}$, where $\text{minmod}\{a, b\} = (\text{sgn}(a) + \text{sgn}(b)) \min\{|a|, |b|\}$. Once the point values (3.8) are recovered and the speeds of propagation (3.9) estimated so as to compute the numerical fluxes (3.7), an evolution routine can be employed to evolve the cell averages of u . We choose a second order SSP Runge-Kutta scheme, [12], for the simulations below,

$$(3.12a) \quad u^{(1)} = u^n + \Delta t C(u^n),$$

$$(3.12b) \quad u^{n+1} = u^{(1)} + \frac{\Delta t}{2} [C(u^{(1)}) - C(u^n)].$$

This scheme is provided by CENTPACK, [1], a software package that implements several central schemes for hyperbolic conservation laws, and we employ it as our base scheme to evolve the solution of (1.1).

3.2. Magnetic and Electric Fields. When L_0 is sufficiently large to ignore the effects of the electron inertia term, T_e , the scheme described above can be used to evolve the solution of the system (1.1) – (1.3) provided the electric field, \mathbf{E} , is approximated consistently with (2.1), and the solenoidal constraint $\nabla \cdot \mathbf{B} = 0$ is enforced. In such cases, we approximate the high-order terms in (2.1) with high-order central finite differences. This allows us to feed back the electric field into the fluxes and evolve the solution of (1.1) with the central scheme described above.

The evolved magnetic field, that we denote by \mathbf{B}^* , is then reprojected onto its divergence free component by solving the Poisson equation,

$$(3.13) \quad \Delta\Phi = -\nabla \cdot \mathbf{B}^*$$

and writing the new magnetic field as

$$(3.14) \quad \mathbf{B}^{n+1} = \mathbf{B}^* + \nabla\Phi.$$

Including the electron inertia term in the description of the electric field poses additional difficulties as it involves the time derivative of \mathbf{j} . For the numerical experiments requiring the approximation of T_e , we have followed two approaches: the finite difference of the the previous two consecutive time values, and the method suggested in [13], where the induction equation is re-written in non-conservative form,

$$(3.15) \quad \frac{\partial \mathbf{B}'}{\partial t} = -\nabla \times \left(\mathbf{v} \times \mathbf{B} + \frac{\mathbf{j} \times \mathbf{B}'}{\rho} + \eta \mathbf{j} \right) + \eta_j \Delta \mathbf{j} \quad \text{with } \mathbf{B}' = \mathbf{B} - \frac{m_e}{m_i} \Delta \mathbf{B}.$$

The first method works only when m_e/m_i is small. For the second method, we build a linear solver using the numerical package Portable Extensible Toolkit for Scientific computation (PETSc).

4. Numerical Result

In order to test the validity of the proposed scheme, we run numerical tests in both linear and non-linear regimes. In the linear regime, we test the dispersion relationship of the system and quantitatively compare the results with analytical solutions. In the non-linear regime, we run a typical reconnection simulation, so that a qualitative comparison of the results obtained can be compared with previous results.

4.1. Dispersion Relationship Test. We begin our numerical experiments by testing the dispersion relation that follows for the linear analysis of the system (1.1) – (1.4) under a small sinusoidal perturbation of wave length λ and amplitude δ . After launching an oscillation with wave length λ in a periodic simulation box, we measure the frequency of the oscillation, and compare the the computed wave speed with the linear analytical prediction.

The linear analysis of the model shows that the wave mode corresponding to the linear polarized Alfvén wave in MHD is a circularly polarized wave known as *whistle* wave (see, for example, [16]). In our numerical test, this wave propagates in the x direction, and the density, pressure and the x components of the velocity and magnetic field remain unperturbed by the small oscillation in both Hall MHD and classic MHD. So the pure Alfvén mode wave will be launched in the simulation domain, no other MHD waves like sonic wave or magnetosonic wave will be triggered.

We evolve the initial conditions

$$(4.1) \quad \begin{aligned} \rho &= 1, & v_x &= 0, & v_y &= -\delta \cos(kx), & v_z &= \delta \sin(kx) \\ p &= 1, & B_x &= 1, & B_y &= \delta v_p \cos(kx), & B_z &= -\delta v_p \sin(kx) \end{aligned}$$

over a solution domain of size $x_L = 9.6$ using a uniform mesh of size $\Delta x = 0.05$, and a perturbation amplitude of $\delta = 10^{-5}$, with periodic boundary conditions. The phase speed v_p is calculated from linear analysis.

We have tested different values of λ corresponding to $m = 2, 8, 15, 24, 30$. The results corresponding to three different versions of the generalized Ohm's law are presented in

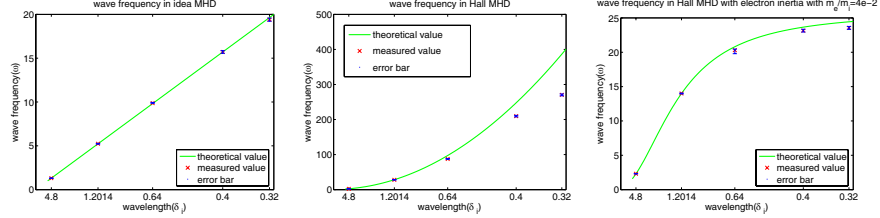


Figure 1: Dispersion relationship for ideal MHD (left), Hall MHD (center), and Hall MHD with electron inertia (right).

The numerical results from classic MHD and Hall MHD with electron inertia simulations are in agreement with the theoretical prediction for wave lengths down to about 6 grid points; at this level the Hall MHD test without electron inertia already displays some discrepancy with theory.

4.2. Reconnection Simulation. Our second experiment is meant to test the effect of the Hall term and electron inertia in the magnetic reconnection phenomenon. Our simulation is similar to the GEM challenge except that we use several boundary conditions.

The initial conditions for this simulation represent a small perturbation of the equilibrium state known as Harris current sheet without guiding field.

The magnetic field, density and pressure profiles are given by

$$(4.2a) \quad B_x(y) = B_0 \tanh(y/\lambda) - \psi_0 y/L_y \cos(2\pi x/L_x) \sin(\pi y/L_y)$$

$$(4.2b) \quad B_y(y) = \psi_0 \cdot 2\pi/L_x \sin(2\pi x/L_x) \cos(\pi y/L_y)$$

$$(4.2c) \quad n(y) = n_0 \operatorname{sech}^2(y/\lambda) + n_b$$

$$(4.2d) \quad p(y) = \frac{1}{2}n(y).$$

where $\psi_0 = 0.1$ is the amplitude of the perturbation, and the velocities are set to zero. In the simulation, we choose $B_0 = 1$ and $n_0 = 1$. The half-width of the current sheet is $\lambda = 0.5$, for the resistivity and hyper-resistivity parameters we choose $\eta = 9 \times 10^{-3}$ and $\eta_j = 1.4 \times 10^{-4}$ respectively, and electron-ion mass ratio is set to $m_e/m_i = 1/25$. The simulation cases have a system size $19.6d_i \times 19.6d_i$ with 639×639 uniform grids.

As for the boundary condition, the GEM challenge has a periodic boundary in the x direction, and conducting wall boundary in the y direction –implemented as in [7] with zero perpendicular current density along the conduction wall.

We also simulate open boundary problems, [8], assuming the simulation box is a region cut from a large background plasma. In the inflow direction an open boundary makes the unperturbed background plasma flow into the simulation domain. And an open boundary allows the plasma that have passed through the reconnection diffusive region flow out the simulation domain without reflection.

In the inflow boundary along the x direction the pressure and density of the plasma remain fixed over time and so does B_x , while B_z is calculated from

$\partial B_z / \partial y = 0$, and B_y from the $\nabla \cdot \mathbf{B} = 0$ condition. The velocity components v_x and v_z are set to zero and v_y is calculated from $\partial v_y / \partial y = 0$. And for the out flow boundary, the pressure, density and v_x are interpolated as $u_{j+1} = 1.3u_j - 0.3u_{j-1}$, B_x is calculated from $\nabla \cdot \mathbf{B} = 0$ condition and B_z , B_y and v_y , v_z obey $\partial u / \partial x = 0$. When electron inertia is included, \mathbf{B}' is assigned according to the same method that is applied on \mathbf{B} . Figure 2 left shows some reflections from the boundary at the beginning of the simulation.

Figures 2 (right) and 3 display the solution computed without electron inertia at time $t = 21\omega_i^{-1}$. The current density profile in 3 indicates that the ratio of the electron diffusive region is in agreement with the reconnection rate as measured by the out of plane electric field in the center of the simulation domain. Figure 5 shows how the reconnection goes into a quasi-steady state at $t = 21\omega_i^{-1}$.

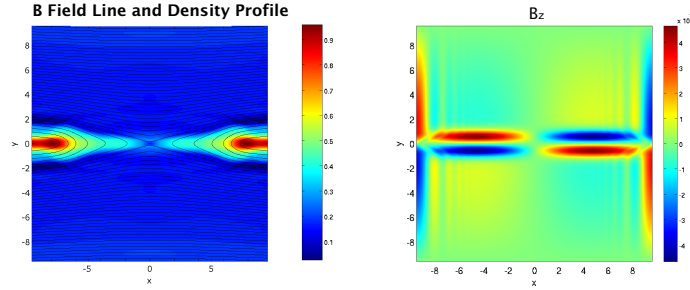


Figure 2: Left: magnetic field lines in quasi steady-state of the reconnection process without electron inertia; Right: out of plane magnetic field at the very beginning stage.

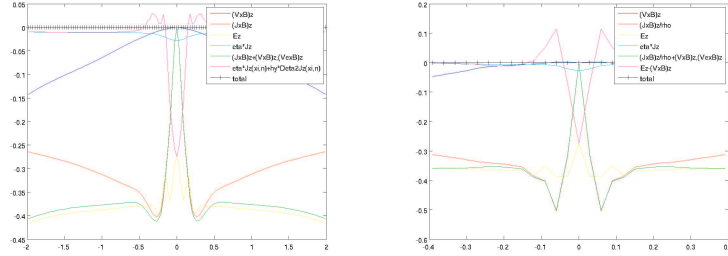


Figure 3: Hall MHD simulation without electron inertia. Left: Terms in the generalized Ohm's law in outflow direction; right: Terms in the generalized Ohm's law in inflow direction.

The simulation with electron inertia also achieves a high reconnection rate (figure 5, right). The current sheet is wider and longer in the simulation with electron inertia than without electron it. This is not only due to the electron inertia term, but also to large dissipation from the large mass of the electrons $1/25$. These results are in agreement with those found in the GEM challenge, [18].

Also, we note that in the center of the diffusive region, we can appreciate a density depletion region, also found in space observations. This suggests that the longitudinal wave might also be important in the Hall MHD simulation, and that it should be included in the Hall MHD simulation both with and without electron inertia.

Our results indicate that central schemes provide a simple, yet robust approach for approximating the solutions of non-classical MHD models with complex wave structures. In the linear regime, the dispersion relationship test shows agreement with the theoretical result. In the nonlinear regime, the reconnection simulation agrees with the previously published result. The numerical package CentPack, [1], allows us to reliably investigate different non-classical MHD models into one numerical code.

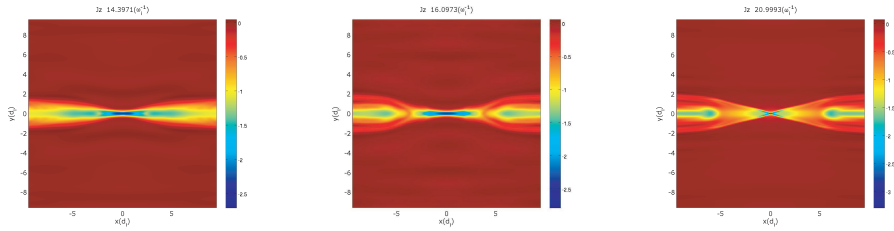


Figure 4: Out of plane current in Hall MHD with electron inertia run at $t = 14.4\omega^{-1}$ (left), $t = 16.1\omega^{-1}$ (center); Out of plane current in Hall MHD without electron inertia run at $t = 21\omega^{-1}$ (right).

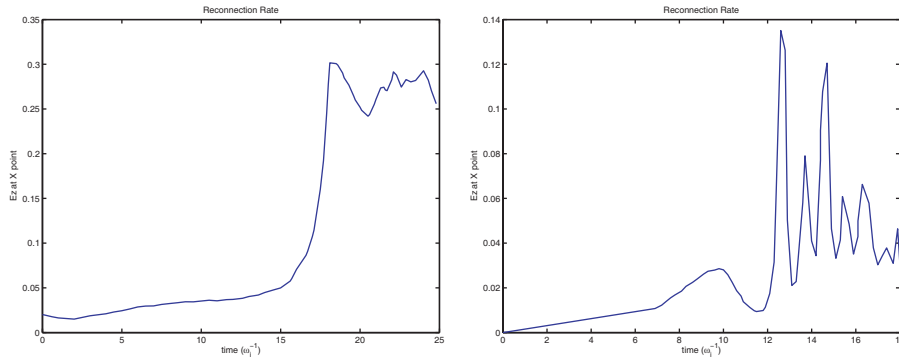


Figure 5: Reconnection rate in Hall MHD simulations. Left: without electron inertia, right: with electron inertia

References

- [1] Jorge Balbás and Eitan Tadmor. CENTPACK. Available for download at <http://www.cscamm.umd.edu/centpack/>, July 2006.
- [2] Jorge Balbás and Eitan Tadmor. Nonoscillatory central schemes for one- and two-dimensional magnetohydrodynamics equations. ii: High-order semidiscrete schemes. *SIAM Journal on Scientific Computing*, 28(2):533–560, 2006.

- [3] Jorge Balbás, Eitan Tadmor, and Cheng-Chin Wu. Non-oscillatory central schemes for one- and two-dimensional MHD equations. I. *J. Comput. Phys.*, 201(1):261–285, 2004.
- [4] N. Bessho and A. Bhattacharjee. Fast collisionless reconnection in electron-positron plasmas. *Physics of Plasmas*, 14(5):056503+, May 2007.
- [5] D. Biskamp. Collisional and collisionless magnetic reconnection. *Physics of Plasmas*, 4:1964–1968, May 1997.
- [6] D. Biskamp, E. Schwarz, and J. F. Drake. Ion-controlled collisionless magnetic reconnection. *Physical Review Letters*, 75(21):3850, November 1995.
- [7] L. Chacón. A non-staggered, conservative, $\nabla b = 0$, finite volume scheme for 3d implicit extended magnetohydrodynamics in curvilinear geometries. *Computer Physics Communications*, 163:143–171, November 2004.
- [8] W. Daughton, J. Scudder, and H. Karimabadi. Fully kinetic simulations of undriven magnetic reconnection with open boundary conditions. *Physics of Plasmas*, 13:2101, July 2006.
- [9] L. Del Zanna, N. Bucciantini, and P. Londrillo. An efficient shock-capturing central-type scheme for multidimensional relativistic flows ii. *Astronomy and Astrophysics.*, 400:397–413, 2003.
- [10] X. H. Deng and H. Matsumoto. Rapid magnetic reconnection in the Earth’s magnetosphere mediated by whistler waves. *Nature*, 410:557–560, March 2001.
- [11] K. Fujimoto. Time evolution of the electron diffusion region and the reconnection rate in fully kinetic and large system. *Physics of Plasmas*, 13:2904, July 2006.
- [12] Sigal Gottlieb, Chi-Wang Shu, and Eitan Tadmor. Strong stability-preserving high-order time discretization methods. *SIAM Rev.*, 43(1):89–112 (electronic), 2001.
- [13] Samuel T. Jones and Scott E. Parker. Including electron inertia without advancing electron flow. *J. Comput. Phys.*, 191(1):322–327, 2003.
- [14] Alexander Kurganov and Eitan Tadmor. New high-resolution central schemes for nonlinear conservation laws and convectiondiffusion equations. *Journal of Computational Physics*, 160:241–282, 2000.
- [15] Z. W. Ma and A. Bhattacharjee. Fast impulsive reconnection and current sheet intensification due to electron pressure gradients in semi-collisional plasmas. *Geophysical Research Letters*, 23:1673–1676, 1996.
- [16] Z. W. Ma and A. Bhattacharjee. Hall magnetohydrodynamic reconnection: The geospace environment modeling challenge. *Journal of Geophysics Research*, 106:3773–3782, March 2001.
- [17] Yang Ren, Masaaki Yamada, Stefan Gerhardt, Hantao Ji, Russell Kulsrud, and Aleksey Kuritsyn. Experimental verification of the hall effect during magnetic reconnection in a laboratory plasma. *Physical Review Letters*, 95(5):055003, 2005.
- [18] M. A. Shay, J. F. Drake, B. N. Rogers, and R. E. Denton. Alfvénic collisionless magnetic reconnection and the Hall term. *Journal of Geophysics Research*, 106:3759–3772, March 2001.
- [19] Bram van Leer. Towards the ultimate conservative difference scheme. V. A second-order sequel to Godunov’s method [J. Comput. Phys. **32** (1979), no. 1, 101–136]. *J. Comput. Phys.*, 135(2):227–248, 1997.

UNIVERSITY OF NEW HAMPSHIRE, DURHAM, NH 03824, USA
E-mail address: xqian@unh.edu

CALIFORNIA STATE UNIVERSITY, NORTHRIDGE, CA 90066, USA
E-mail address: jorge.balbas@csun.edu

UNIVERSITY OF NEW HAMPSHIRE, DURHAM, NH 03824, USA
E-mail address: amitava.bhattacharjee@unh.edu

UNIVERSITY OF NEW HAMPSHIRE, DURHAM, NH 03824, USA
E-mail address: hongang.yang@unh.edu